

## Binding Interactions of Nucleobase-substituted Ponatinib Analogues with Wild-type and T315I BCR-ABL Tyrosine Kinases

Vince Lambert H. Padilla<sup>1,2,\*</sup> and Glenn V. Alea<sup>2</sup>

<sup>1</sup> Department of Pharmaceutical Chemistry, College of Pharmacy, University of the Philippines Manila

<sup>2</sup> Department of Chemistry, College of Science, De La Salle University

\*Corresponding Author: [vince.padilla@dlsu.edu.ph](mailto:vince.padilla@dlsu.edu.ph), [vhpadilla@up.edu.ph](mailto:vhpadilla@up.edu.ph)

**Abstract:** Ponatinib (AP24534), a chemotherapeutic agent used to treat chronic myeloid leukemia, exhibits its action through the competitive inhibition of BCR-ABL tyrosine kinases. Despite its potency towards resistant variants of the enzyme including the T315I mutant, compound point mutations in the Philadelphia chromosome still led to the formation of ponatinib-resistant kinases. To provide a better understanding of the binding pockets of the wild-type and T315I kinases, molecular docking simulations of adenine-, guanine-, cytosine-, uracil-, and thymine-substituted ponatinib towards PDB models 3CS9 and 3OY3 were performed. Among the nine analogues, five have exhibited binding free energies comparable to ponatinib (-14.49<sup>3CS9</sup>, -15.55<sup>3OY3</sup>), with A-N9 (-14.69<sup>3CS9</sup>, -16.42<sup>3OY3</sup>) being the closest. The other analogues — G-C8, G-N9, U-M1, and T-M1 — were found to have significantly weaker binding towards one of the models used; the latter three bound to the 3OY3 pocket in an entirely different orientation. Various interactions of the ligands with 31 amino acid residues in the binding pocket have been detected.

**Key Words:** BCR-ABL; tyrosine kinase inhibitors; purines; pyrimidines; molecular docking

### 1. INTRODUCTION

The Breakpoint Cluster Region – Abelson (BCR-ABL) fusion tyrosine kinase is the main oncoprotein responsible for malignancies in Chronic Myeloid Leukemia (CML). It is a fusion protein resulting from the reciprocal t(9;22)(q34;q11) translocation wherein the part of the ABL gene responsible for the autoregulation of its kinase activity is replaced by the breakpoint cluster region (Colicelli, 2010). Ponatinib is a 3<sup>rd</sup> generation BCR-ABL tyrosine kinase inhibitor that occupies the ATP-binding pocket of the enzyme. Like the 1<sup>st</sup> gen TKI imatinib and 2<sup>nd</sup> gen TKI nilotinib, ponatinib competes with ATP and binds while the enzyme is in its DFG-out conformation. This allows the molecules

to interact with various parts of the binding region including the formation of hydrogen bonds (H-bonds) with M318, D381, E286, I360, and H361 (Fig. 1). Imatinib and nilotinib can form another H-bond with the gatekeeper residue T315. However, these drugs lose their affinity towards the T315I mutant where isoleucine replaces threonine at position 315, thereby causing the gatekeeper residue to sterically repel the 1<sup>st</sup> and 2<sup>nd</sup> generation inhibitors (Reddy & Aggarwal, 2012). Ponatinib evades this resistance mechanism due to its non-bulky ethynyl moiety that also serves as a rigid linker of its imidazo[1,2-*b*]pyridazine and benzamide rings.

The discovery of newer inhibitors of this class is driven by the development of resistance against the prototype and older drugs. Ponatinib, for example,

was designed to inhibit the BCR-ABL kinase T315I mutant since its predecessors are unable to inhibit this enzyme (Huang et al., 2010). Despite the high potency of ponatinib against the wild-type and several mutants of BCR-ABL kinase, treatment challenges still arise because of severe cardiovascular toxicity cases experienced by some patients who took the drug (Azanza et al., 2018). There are also some cases in which ponatinib resistance is observed due to compound point mutations in key domains of the target enzyme (Zabriskie et al., 2014). With these challenges, the researchers aim to provide more insights on how various modifications in the structure of ponatinib would affect its interactions with the binding residues of wild-type and T315I BCR-ABL tyrosine kinases. Constrained type molecular docking — where the ligands are flexible while the target proteins are rigid (Silakari & Singh, 2021) — was utilized to generate the bound conformations of the ponatinib analogues that were analyzed in this study.

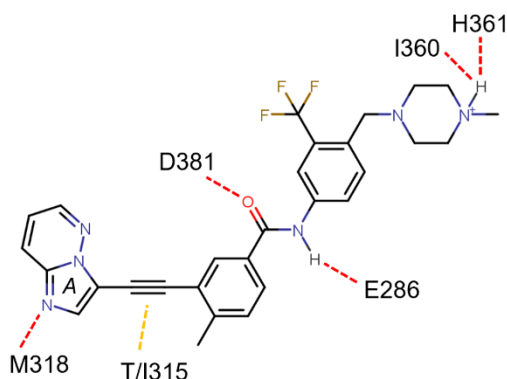


Fig. 1. Ponatinib with some key interacting residues in the ATP-binding site of BCR-ABL kinase

## 2. METHODOLOGY

### 2.1. Preparation of Protein Files

Appropriate *.pdb* models of the BCR-ABL tyrosine kinases in their DFG-out conformations were downloaded from the RCSB Protein Data Bank (PDB) (<https://www.rcsb.org>). PDB ID 3CS9 (Weisberg et al., 2005) and 3OY3 (Zhou et al., 2011) were used as the models for the wild-type and T315I mutant proteins, respectively. For each *.pdb* file, water molecules were first deleted. Out of 4 repeating chains in 3CS9, only Chain A was retained due to its superior quality over chains B to D. As for 3OY3 which contains 2 repeating units, Chain A was used due to the same reason. No metal ions were present in both models. Their

respective ligands were deleted to empty the binding site. All possible hydrogens were then added to the structure, followed by the merging of nonpolar hydrogens. After adding hydrogens, the acidic groups of Glu and Asp residues remained as carboxylates while the basic groups of Lys, Arg, and His were in their +1 protonated forms. Lastly, Kollman charges were added and the files were saved as *.pdbqt* filetype. AutoDockTools (ADT) 1.5.6 was used for the entire protein preparation step.

### 2.2. Preparation of Ligand Files

The 2D chemical structures of the analogues and controls were drawn using the 2018 Freeware version of ACD/ChemSketch. All structures containing the *N*-methylpiperazine moiety were drawn in their *N4* protonated forms. The initial conformations were optimized using *Clean Structure*, *Add Explicit Hydrogens*, and *3D Optimization*, then saved as *.mol* filetypes. On the other hand, the native ligands of the chosen protein models were also prepared. Using ADT, nilotinib and AP24589 were extracted as *.pdbqt* files from 3CS9 and 3OY3, respectively, then converted to *.mol* with Open Babel 2.4.1. They were opened in ChemSketch for the addition of explicit hydrogens and *3D Optimization*, then saved as new *.mol* files.

All *.mol* files were converted to *.mol2* filetypes, then opened in ADT 1.5.6 as ligands for the merging of nonpolar hydrogens, addition of Gasteiger charges, and selection of rotatable bonds. The processed ligands were saved as *.pdbqt* files.

### 2.3. Molecular Docking Simulations

In ADT, the grid boxes were positioned to sufficiently cover the ATP-binding site. A 46 by 44 by 34 grid box centered at 28.375X–4.103Y–51.782Z was used for 3CS9, while a 62 by 34 by 28 box at 16.540X–6.904Y–2.762Z was used for 3OY3. The default 0.375 Å spacing for each grid point was used in both models. Grid calculations for each ligand-protein pair were followed by docking calculations using AutoDock 4.2.6, where Lamarckian Genetic Algorithm (GA) was used in searching for the best conformations of the ligands. The number of GA runs was set to 500 while all other parameters were set to default. ADT and BIOVIA Discovery Studio Visualizer v21.1.0.20298 (BIOVIA Dassault Systèmes, 2020) were then used for viewing, calculation of root-mean-square deviation (RMSD), and detection of ligand-protein interactions.

### 3. RESULTS AND DISCUSSION

#### 3.1. Validation of Docking Parameters

Redocking of the extracted nilotinib and AP24589 were performed to assess the validity of the entire docking process. The goal is to reproduce the same pose of the native ligand in the downloaded PDB model. Specifically, the closeness of the redocked ligand to that of the native ligand was measured in terms of RMSD.

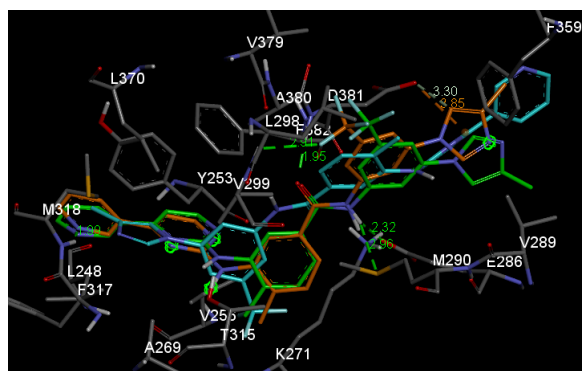


Fig. 2. Superimposed conformations of native and redocked nilotinib in 3CS9

In 3CS9, the resulting 500 conformations of nilotinib were automatically grouped by ADT into 15 clusters based on their binding free energies and RMSDs. The top conformer (Fig. 2, orange) with a binding energy of  $-14.49$  kcal/mol was calculated to have an RMSD of  $1.211$  Å in reference to the native pose (green). Their interactions with the binding residues in the active site are also similar. The top conformer interacts with 19 residues as shown in the figure, while the native pose has interactions with only 18 residues. Both exhibit the known H-bonds with T315, M318, E286, and D381, as well as various pi, halogen, and alkyl interactions with 13 other residues. L298, F359, and V379 interact solely with the top conformer, while the native pose has exclusive interactions with K285 and H361. These variations can be attributed to the slightly different orientations of their methylimidazole rings. Additionally, a binding pose with an entirely different orientation (cyan) is also possible. This conformer from cluster 5 has a binding energy of  $-11.19$  kcal/mol and an RMSD of  $12.067$  relative to the native pose. Despite the different orientations and similar cluster size of the top cluster (27.6%) and cluster 5 (31.2%), the docking procedure is still considered valid for the wild-type

protein since cluster 1 poses are more energetically favorable than the other, even after considering the 2-3 kcal/mol standard error of AutoDock4 (Morris et al., 2009).

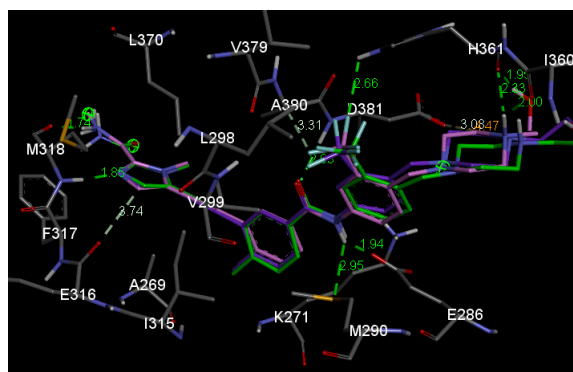


Fig. 3. Superimposed conformations of native and redocked AP24589 in 3OY3

As for the T315I mutant, two forms of AP24589 were redocked into the binding site of 3OY3. Relative to the native pose (Fig. 3, green), the calculated RMSDs are  $0.826$  Å for the free base (purple) and  $1.218$  Å for the methylpiperazine *N*-protonated form (magenta). The latter has a total of 16 interactions including the known H-bonds with M318, E286, D381, I360, and H361, and has a free binding energy of  $-16.04$ . On the other hand, while the free base ( $-15.47$  kcal/mol) lacks the H-bonding of the methylpiperazine with I360 and H361, a new H-bond with I360 was observed through its hydroxyethyl substituent. Aside from H361, the protonated form has an exclusive interaction with E316, while the free base interacts with V256. The interactions are also similar to that of the native conformer except those with V299 which was only observed in the redocked conformers, and those with I293 which was only found in the native. With these RMSDs, interactions, energies, and top cluster sizes for both the free base (84.0%) and the protonated AP24589 (91.0%), the docking procedure for the T315I mutant is also considered valid.

#### 3.2. Binding of Existing BCR-ABL Tyrosine Kinase Inhibitors

Molecular docking simulations using ponatinib and its predecessors — imatinib and nilotinib — were performed to survey possible modes of interactions and interacting residues to monitor. Fig. 4 shows the binding pocket residues of the wild-

type and T315I BCR-ABL kinases that interact with the *N4*-protonated ponatinib. On top of the known H-bonding residues shown in Fig. 1, 14 other residues were observed to contribute to the binding of the ligand. These are L248, Y253, A269, K271, M290, L298, V299, E316, F317, R362, L370, V379, A380, and F382. Interactions with these residues are all beneficial except for R362 in which possible repulsive forces have been observed between its guanidino group and the piperazinyl moiety of ponatinib, both of which are positively charged.

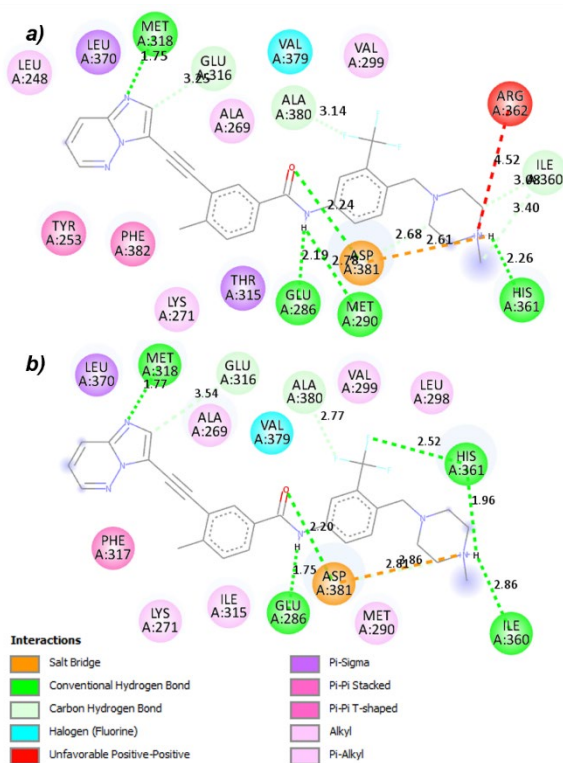


Fig. 4. Interactions of Ponatinib in the ATP-binding sites of a) 3CS9 and b) 3OY3

Similar to what was reported in several articles (Reddy & Aggarwal, 2012; Rossari et al., 2018; Tanneeru & Guruprasad, 2013), the following weak to moderate H-bonds have been observed: M318 NH with the imidazo[1,2-*b*]pyridazine N (moderate), E286 carboxylate with the amide linker NH (moderate), D381 amide NH with the amide linker O (weak), and the amide O's of I360 (weak) and H361 (moderate) with the NH of the protonated methylpiperazine. In the 3OY3 model, the H361 imidazole can also serve as a weak H-bond donor to the fluorine substituents. In 3CS9, a weak H-bond between M290 S and the amide

linker NH was detected. Aside from its H-bond with the amide linker, D381 is also able to form an ionic bridge with the protonated methylpiperazine through its carboxylate group. The corresponding strengths of the H-bonds were based on the ranges by Grabowski (2020) where H...acceptor distances of  $\sim 1.2$  to  $\sim 1.5$  Å are strong,  $\sim 1.5$  to  $\sim 2.2$  Å are moderate, and  $\sim 2.2$  to  $\sim 3.2$  are weak.

Aromatic pi interactions of the imidazo[1,2-*b*]pyridazine with aromatic residues in the binding site were also detected — a stacked pi-pi interaction with 3CS9 F382, a T-shaped pi-pi interaction with 3CS9 Y253, and a stacked pi-pi interaction with 3OY3 F317. Pi-alkyl interactions between the ponatinib aromatic rings and L248, A269, K271, M290, and I315 of the binding pocket have also been observed. Since I315 is a threonine residue in the wild-type model, the interaction between this position and the benzamide moiety of ponatinib is pi-sigma in nature. Lastly, the trifluoromethyl moiety was observed to have a pi-alkyl interaction with the imidazole ring of H361, alkyl interactions with the side chains of L298, V299, and V379, halogen interactions with the carbonyls of V379 and A380, and intramolecular halogen interactions with *N1* of the methylpiperazine.

As for imatinib and nilotinib, both ligands formed weak (3.06 Å) and moderate (1.96 Å) H-bonds with T315 through their guanidino NH, respectively, on top of the aforementioned interactions of this nature. Their pyridine and pyrimidine rings can form pi-pi interactions with Y253, F317, and F382, pi-sigma interactions with L248, A269, and L370, and pi-alkyl interactions with L248, V256, A269, and L370. Pi-anion interactions can be formed by the D381 carboxylate with the benzamide ring of imatinib or with the methylimidazole of nilotinib. The latter can also form T-shaped pi-pi interactions with the aromatic rings of H361 and F359.

### 3.3. Binding of Purine-substituted Ponatinib Analogues

Nine analogues of ponatinib were generated by substituting the imidazo[1,2-*b*]pyridazine ring system with the nucleobases Adenine, Guanine, Cytosine, Uracil, and Thymine (Fig. 5). The purines were attached to the ethynyl linker either through the *N9* or *C8* positions while the pyrimidines were connected either through *N1* or *C5*, except for Thymine which cannot be substituted at the latter due to its methyl group at position 5.

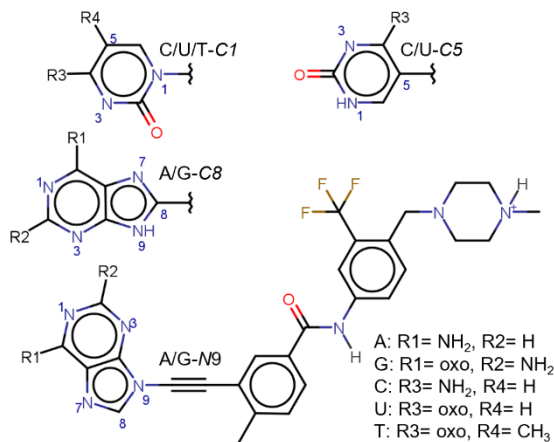


Fig. 5. 2D structures of purine- and pyrimidine-substituted ponatinib analogues

The lowest binding energies out of 500 generated poses for each ligand are shown in Table 1. The adenine M9-attached analogue (A-M9) has shown the most negative free binding energies among all analogues in both models, while the G-C8 and U-M1 exhibited the least negative scores in the wild-type and T315I models, respectively. Taking the AD4 standard error of 2-3 kcal/mol into account (Morris et al., 2009), only G-C8 has a significantly weaker affinity than ponatinib in the 3CS9 pocket, whereas G-M9, U-M1, and T-M1 have weaker affinities towards the 3OY3 pocket. The rest of the analogues can be considered to have comparable affinities to that of ponatinib.

Table 1. Binding profiles of nucleobase-substituted ponatinib analogues

Ligand	Binding Energy (kcal/mol)		Interacting Residues	
	3CS9	3OY3	3CS9	3OY3
Ponatinib	-14.49	-15.55	18	16
A-M9	-14.69	-16.42	16	17
A-C8	-13.49	-14.71	16	16
G-M9	-12.93	-12.20	17	13
G-C8	-11.38	-15.14	17	17
C-M1	-13.23	-15.82	15	16
C-C5	-13.67	-15.80	19	17
U-M1	-12.75	-11.81	17	12
U-C5	-12.64	-14.75	20	16
T-M1	-13.28	-11.98	15	12

The energies of A-M9 may be attributed to its 6-amino group which serves as a donor to the H-bond acceptor carbonyl O of M318 (weak). The dashed green and orange lines shown in Fig. 6 represent the H-bond

and electrostatic interactions of A-M9 (magenta) with the binding pocket, which are almost the same as those of ponatinib (white). Exceptions are the alkyl and halogen interactions of ponatinib with V299 and V379 of 3CS9, and the pi-alkyl interaction of A-M9 with L248 of 3OY3. In the case of A-C8 (cyan), the C8-attached adenine is oriented differently to allow moderate H-bonding between its N3 and M318 NH, and a weak H-bond between its 6-amino group and the phenol O of Y253. The latter, however, was only detected in the wild-type model. The benzoyl moieties of both A-M9 and A-C8 are almost coplanar with that of the parent compound. The phenylamine moieties and the methylene linkers are oriented in a slightly different manner which appears to be driven by weak H-bond interactions between the trifluoromethyl F and the imidazole NH of H361.

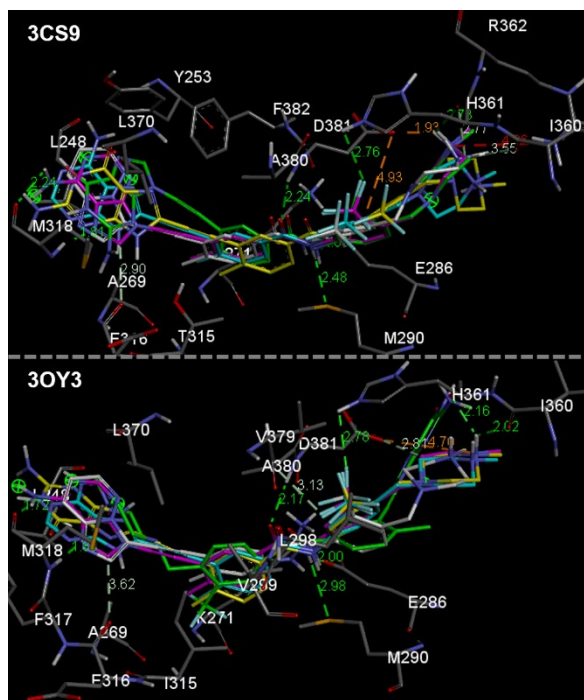


Fig. 6. Superimposed top conformers of purine-substituted ponatinib analogues

The guanine-substituted analogues showed relatively poorer free binding energies than their adenine counterparts except for G-C8 (yellow) in the T315I model. This analogue is bound to the 3OY3 pocket in such a way that the center of its purine core is matched to the center of the 6-membered components of the bicyclic systems of A-M9 and ponatinib. While this resulted in an off-angled ethynyl linker, it allows the guanine moiety to form a

moderate H-bond between its 6-oxo and the M318 NH, and stacked pi-pi interactions with F317. Its trifluoromethyl F also formed a weak H-bond with the H361 imidazole NH. On the other hand, G-C8 bound differently in the 3CS9 pocket where its 2-amino and N9-H served as donors to the H-bond accepting carbonyls of M318 (moderate) and E316 (weak). Such interactions, however, resulted to an offset where the molecule appears pushed towards the region near I360 and H361, thereby disrupting the possible H-bonds of its methylpiperazine with the said residues.

Table 2. Types of favorable interactions formed by the analogues with the targets

Ligand	No. of Interactions					
	H-Bonds <sup>a</sup>		Electrostatic		Others <sup>b</sup>	
	3CS9	3OY3	3CS9	3OY3	3CS9	3OY3
Pon	5 (5)	6 (3)	1	1	16	18
A-M9	7 (3)	8 (3)	2	1	15	17
A-C8	5 (4)	7 (3)	1	1	15	20
G-M9	7 (2)	8 (0)	2	2	20	12
G-C8	5 (3)	7 (1)	2	1	14	18
C-M1	5 (3)	9 (2)	2	1	13	16
C-C5	8 (3)	9 (2)	1	1	15	17
U-M1	1 (4)	5 (1)	1	0	14	15
U-C5	3 (5)	9 (3)	1	1	17	15
T-M1	4 (3)	6 (1)	1	0	11	16

<sup>a</sup> enclosed in parentheses are non-classical H-bonds

<sup>b</sup> hydrophobic, halogen, & miscellaneous interactions

As for G-M9 (green), the N1-H and 2-amino groups formed weak and moderate H-bonds with the M318 and E316 carbonyls, respectively, in the 3CS9 pocket. This led to an off-angled ethynyl linker and the loss of a pi-sigma interaction between the benzoyl ring and T315. Lastly, the docked G-M9 in the 3OY3 pocket is in an entirely different orientation relative to the poses of ponatinib and all previously discussed analogues. The methylpiperazine is positioned in the pocket that receives the imidazo[1,2-*b*]pyridazine, where it lacks any interaction with the surrounding residues. The phenylamine moiety is in the position of benzoyl which forms weak H-bond interactions from the I315 and K271 NH to the trifluoromethyl F's. The benzoyl moiety is oriented in a manner where the ethynyl linker places guanine in a new pocket beside the binding site for methylpiperazine. In this pocket, guanine forms weak and moderate H-bonds with the R386 guanidine through its 6-oxo group, and with the H361 carbonyl O through its 2-amino group (weak). Pi-anion interactions were also detected between guanine and the carboxylates of E282 and D381. These interactions are summarized in Table 2.

### 3.4. Binding of Pyrimidine-substituted Ponatinib Analogues

Among the pyrimidine-substituted analogues, C-C5 (Fig. 7, cyan) and C-M1 (magenta) have shown the best binding free energies in the wild-type and T315I models, respectively (Table 1). Similar to its adenine counterpart, C-M1 can form moderate to weak H-bonds with M318 through its N3 and 4-amino positions, while C-C5 forms moderate H-bonds with M318 also through N3 then with the E316 carbonyl through its 4-amino group. Pi-pi interactions between cytosine and the aromatic rings of Y253, F317, and F382 were detected for both analogues but are more evident in C-C5.

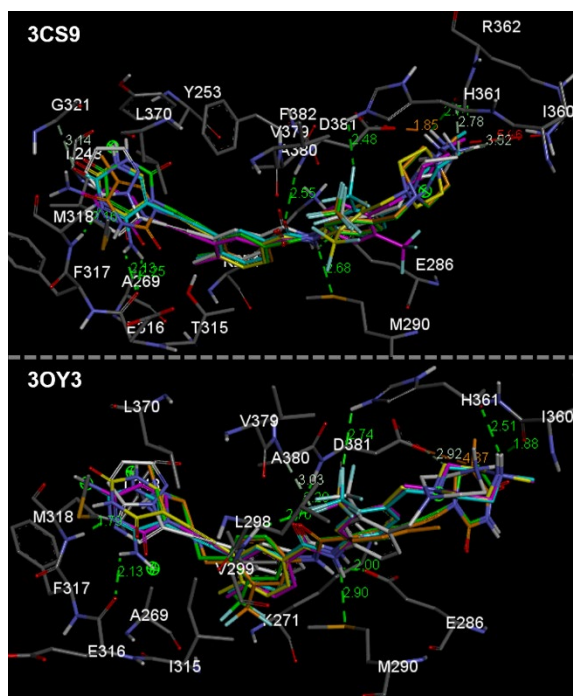


Fig. 7. Superimposed top conformers of pyrimidine-substituted ponatinib analogues

While the benzoyl moiety and amide linker interactions are the same as those of ponatinib, the phenylamine moiety can form additional interactions. In the 3CS9 pocket, the phenylamine of C-M1 is flipped in such a way that its trifluoromethyl group is on the other ortho-position of the ring and is oriented towards V289, forming several alkyl and halogen bonds with nearby substituents. This conformation appears to be stabilized by an intramolecular attraction between N1 of the piperazine and the

halogens of trifluoromethyl. The phenylamine of C-M1 in 3OY3 and of C-C5 in both models are slightly tilted but their trifluoromethyls are still on the same side as that of ponatinib, allowing weak H-bonding with the imidazole NH of H361. Another weak H-bond was detected between these halogens and V299 NH of the 3OY3 pocket.

The 3CS9-bound U-M1 (green) has its uracil H-bonding moieties oriented away from the side of M318, hence only pi interactions were observed. Its methylated counterpart T-M1 (orange) was able to form the moderate and weak H-bonds with Met318 and Glu316 through its 4-oxo and N3-H, plus an additional weak H-bond between its 2-oxo and the T315 OH. As for their counterparts in the 3OY3 model, the analogues were docked in a similar manner as G-M9 which resulted to less interactions when compared to the other pyrimidine analogues (Table 2). In these poses, the methylpiperazines are positioned near M318 while the pyrimidine cores are oriented towards E282. The carboxylate of this residue can form moderate H-bond interactions with the N3-H of both analogues. Ile315 and K271 are also able to form weak H-bonds with the trifluoromethyl groups of these conformers. On the other hand, U-C5 (yellow) binds inside both models via the usual orientation. While its 4-oxo and 2-oxo are able to form weak H-bonds with M318 and G321, possible donor-donor repulsions between its N3-H and M318 NH, as well as acceptor-acceptor repulsions between its 4-oxo and M318 carbonyl were detected. The rest of the molecule interacts similarly as its cytosine counterpart.

#### 4. CONCLUSIONS

Redocking of the native ligands of PDB models 3CS9 and 3OY3 resulted in conformers having RMSDs of less than 2.0 Å relative to their native poses. The process was then applied to the molecular docking simulations of ponatinib and nine nucleobase-substituted analogues. Most analogues exhibited binding free energies comparable to the scores of ponatinib except for G-C8 which was found to have a significantly weaker affinity towards the wild-type model, as well as G-M9, U-M1, and T-M1 towards the T315I model. The latter three even bound in an entirely different manner. Various ionic, pi, halogen, alkyl, and weak to moderate H-bond interactions between the ligands and 31 residues in the binding site were detected. These residues are E286, T315, I315, M318, I360, H361, D381, Y253, K271, E282, M290, V299, E316, G321, R386, F317,

F359, F382, L248, V256, A269, V270, V289, I293, L298, I313, I314, L370, V379, A380, and R362.

Structural modifications — individual and combined — in other parts of ponatinib have also been performed but were not included in this paper. Synthesis of selected analogues are also underway. Moving forward, the synthesized analogues can be subjected to BCR-ABL tyrosine kinase inhibition and cell-based assays to assess the actual effects of such modifications. On top of those that were initially generated, additional analogues may also be designed specifically to optimize the interactions described in this paper.

#### 5. ACKNOWLEDGMENTS

The authors would like to acknowledge the DLSU Department of Chemistry, the NSYSU Chemistry Department, especially Prof. Chun-Hu Chen, and the UP Manila College of Pharmacy for taking part in the collaborative research from which this paper was derived.

#### 6. REFERENCES

- Azanza, J. R., Sádaba, B., & Díez, N. (2018). Comparative Pharmacology of Tyrosine Kinase Inhibitors for the Treatment of Chronic Myeloid Leukemia. *International Journal of Clinical Pharmacology & Pharmacotherapy*, 3(134), 1–15. <https://doi.org/10.15344/2456-3501/2018/134>
- BIOVIA Dassault Systèmes. (2020). *Discovery Studio Visualizer* (v21.1.0.20298). Dassault Systèmes. <https://discover.3ds.com/discovery-studio-visualizer-download>
- Colicelli, J. (2010). ABL tyrosine kinases : Evolution of Function , Regulation , and Specificity. *Science Signaling*, 3(139), 1–26. <https://doi.org/10.1126/scisignal.3139re6>
- Grabowski, S. J. (2020). Chapter 1. Hydrogen Bond – Definitions, Criteria of Existence and Various Types. In *Understanding Hydrogen Bonds: Theoretical and Experimental Views* (pp. 1–40). Royal Society of Chemistry. <https://doi.org/10.1039/9781839160400-00001>
- Huang, W. S., Metcalf, C. A., Sundaramoorthi, R., Wang, Y., Zou, D., Thomas, R. M., Zhu, X., Cai, L., Wen, D., Liu, S., Romero, J., Qi, J., Chen, I., Banda, G., Lentini, S. P., Das, S., Xu, Q., Keats,

- J., Wang, F., ... Shakespeare, W. C. (2010). Discovery of 3-[2-(imidazo[1,2-b]pyridazin-3-yl)ethynyl]-4-methyl-N-{4-[(4-methylpiperazin-1-yl)methyl]-3-(trifluoromethyl)phenyl}benzamide (AP24534), a potent, orally active pan-inhibitor of breakpoint cluster region-abelson (BCR-ABL) kinase includin. *Journal of Medicinal Chemistry*, *53*(12), 4701–4719. <https://doi.org/10.1021/jm100395q>
- Morris, G. M., Huey, R., Lindstrom, W., Sanner, M. F., Belew, R. K., Goodsell, D. S., & Olson, A. J. (2009). AutoDock4 and AutoDockTools4: Automated Docking with Selective Receptor Flexibility. *Journal of Computational Chemistry*, *30*, 2785–2791.
- Reddy, E. P., & Aggarwal, A. K. (2012). The Ins and Outs of Bcr-Abl Inhibition. *Genes and Cancer*, *3*(5–6), 447–454. <https://doi.org/10.1177/1947601912462126>
- Rossari, F., Minutolo, F., & Orciuolo, E. (2018). Past, present, and future of Bcr-Abl inhibitors: from chemical development to clinical efficacy. *Journal of Hematology & Oncology*, *11*(84), 1–14. <https://doi.org/10.1186/s13045-018-0624-2> REVIEW
- Silakari, O., & Singh, P. K. (2021). Molecular docking analysis: Basic technique to predict drug-receptor interactions. In *Concepts and Experimental Protocols of Modelling and Informatics in Drug Design* (pp. 131–155). <https://doi.org/10.1016/b978-0-12-820546-4.00006-4>
- Tanneeru, K., & Guruprasad, L. (2013). Ponatinib is a pan-BCR-ABL kinase inhibitor: MD simulations and SIE study. *PLoS ONE*, *8*(11). <https://doi.org/10.1371/journal.pone.0078556>
- Weisberg, E., Manley, P. W., Breitenstein, W., Brügger, J., Cowan-Jacob, S. W., Ray, A., Huntly, B., Fabbro, D., Fendrich, G., Hall-Meyers, E., Kung, A. L., Mestan, J., Daley, G. Q., Callahan, L., Catley, L., Cavazza, C., Mohammed, A., Neuberg, D., Wright, R. D., ... Griffin, J. D. (2005). Characterization of AMN107, a selective inhibitor of native and mutant Bcr-Abl. *Cancer Cell*, *7*(2), 129–141. <https://doi.org/10.1016/j.ccr.2005.01.007>
- Zabriskie, M. S., Eide, C. A., Tantravahi, S. K., Vellore, N. A., Estrada, J., Nicolini, F. E., Khoury, H. J., Larson, R. A., Konopleva, M., Cortes, J. E., Kantarjian, H., Jabbour, E. J., Kornblau, S. M., Lipton, J. H., Rea, D., Stenke, L., Barbany, G., Lange, T., Hernández-Boluda, J. C., ... O'Hare, T. (2014). BCR-ABL1 Compound Mutations Combining Key Kinase Domain Positions Confer Clinical Resistance to Ponatinib in Ph Chromosome-Positive Leukemia. *Cancer Cell*, *26*(3), 428–442. <https://doi.org/10.1016/j.ccr.2014.07.006>
- Zhou, T., Commodore, L., Huang, W. S., Wang, Y., Thomas, M., Keats, J., Xu, Q., Rivera, V. M., Shakespeare, W. C., Clackson, T., Dalgarno, D. C., & Zhu, X. (2011). Structural Mechanism of the Pan-BCR-ABL Inhibitor Ponatinib (AP24534): Lessons for Overcoming Kinase Inhibitor Resistance. *Chemical Biology and Drug Design*, *77*(1), 1–11. <https://doi.org/10.1111/j.1747-0285.2010.01054.x>